9 Radiative Transfer in the Coupled Atmosphere-Snow-Ice-Ocean (CASIO) System: Review of Modeling Capabilities

Knut Stamnes[1], Børge Hamre[2], and Jakob J. Stamnes[2]

[1] Light and Life Laboratory, Department of Physics and Engineering Physics, Stevens Institute of Technology, Hoboken, NJ 07030, USA
E-mail: Knut.Stamnes@stevens.edu
[2] Department of Physics and Technology, University of Bergen, Postboks 7800, 5020 Bergen, Norway
E-mail: Børge.Hamre@ift.uib.no
E-mail: Jakob.Stamnes@ift.uib.no

Abstract A review is provided of ultraviolet (UV) and visible radiative transfer in an atmosphere-sea-ice-ocean system with emphasis on the basic physical principles involved rather than on mathematical/numerical techniques. To illustrate the application of the theory, a few examples are provided. First, we provide a comparison of two different models for radiation penetration into the open ocean, which for a given set of input parameters give identical results. Thus, for a stratified atmosphere-ocean system, our ability to model the transfer of UV radiation and visible light appears to be limited as much by reliable information about the inherent optical properties of marine constituents as by our ability to accurately solve the radiative transfer equation. Second, we discuss a comparison between measured and modeled radiative transfer results in an atmosphere-sea ice-ocean system, which reveals that accurate transmittances as well as accurate values for the radiative energy deposition versus depth can be calculated. Third, we review results of a study showing that multiple scattering in a highly scattering medium such as sea ice gives rise to a marked enhancement of the downward irradiance across the atmosphere-sea ice interface. Finally, we review a recent study in which the modeled radiation field is used to illustrate how the primary production in icy polar waters might be influenced by an ozone depletion. Contrary to previous investigations, this study reveals that a 50% ozone depletion might lead to an increase (~1%) rather than a decrease in primary productivity.

Keywords UV radiation modeling, photolysis, actinic flux, atmospheric warming/cooling rates, UV radiation in aquatic systems

9.1 Introduction

The bulk of the earth's atmosphere (99% by mass) consists of molecular nitrogen and oxygen, which are homonuclear, diatomic molecules that absorb little radiation at wavelengths in the UV and visible spectral ranges. Trace amounts of polyatomic molecules including ozone are responsible for atmospheric absorption. In recent years, ozone loss has been tied to the release of man-made trace gases, mainly chlorofluorocarbons used in the refrigeration industry and as propellants in spray cans. Because ozone provides an effective shield against harmful UV solar radiation, a thinning of the ozone layer due to release of man-made trace gases (Solomon, 1990; Anderson et al., 1991) could have serious biological ramifications (Slaper et al., 1995; Herman et al., 1996; Zerefos and Bais, 1997; Herman et al., 1999).

UV radiation (280 nm – 400 nm) and visible solar radiation determine the concentration of *photochemically active* species through the process of *photolysis*, in which molecules are split up into atoms and smaller molecules. Here we assume for convenience that visible radiation is approximately equal to photosynthetically active radiation (PAR, 400 nm – 700 nm). Ozone is formed when an oxygen atom (O) and an oxygen molecule (O_2) combine to yield O_3. Chemical reactions and photolysis are responsible for the destruction of atmospheric ozone. The bulk content of the ozone gas residing in the stratosphere is determined by a balance between these production and loss processes.

UV radiation penetrating to the troposphere and surface is customarily divided into two spectral ranges: UV-B (280 nm – 320 nm) and UV-A (320 nm – 400 nm). Living organisms are much more susceptible to damage by UV-B radiation than by the more benign UV-A radiation. Fortunately, UV-B radiation is very effectively absorbed by ozone, and therefore very sensitive to the total column amount of O_3.

As a result of stratospheric ozone depletion, UV-B radiation (280 nm – 320 nm) is likely to increase and have adverse effects on both individual marine organisms and marine ecosystems (Worrest, 1986; Holm-Hansen et al., 1993a; Cullen and Neale, 1994; Prézelin et al., 1994; Häder et al., 1998), because UV-B radiation can penetrate to ecologically significant depths in the ocean (Smith and Baker, 1989; Zeng et al., 1993). Many marine organisms are sensitive to UV-B radiation, and it remains uncertain whether or not they will be able to adapt to increases in UV-B radiation exposure (Karentz et al., 1991; 1992). Numerous investigations (Calkins and Thordardottir, 1980; Worrest, 1986; Smith et al., 1992; Holm-Hansen et al., 1993b, Wängberg et al., 1999) have provided indications that UV-B radiation influences phytoplankton productivity. Calkins and Thordardottir (1980) argued that UV radiation is a significant ecological factor, and Jokiel and York (1984) linked long-term growth inhibition to UV radiation. Worrest (1986) found that acute exposure to UV-B radiation significantly depressed primary productivity. Damaging effects on other metabolic processes of phytoplankton and microorganisms have been studied by several groups (Döhler, 1985; Neale et al., 1993; Goes et al., 1995), and recent studies have included effects of UV radiation on pigments and

assimilation of inorganic nitrogen (Döhler and Hagmeier, 1997; Lobman et al., 1998).

Penetration of UV radiation and visible light in the ocean is strongly influenced by small plankton and thus, by biological productivity which provides a close link between biological and optical oceanography (Smith and Baker, 1989). Important aspects of the ozone depletion issue include the effects of increased UV radiation levels on algae, plankton, and fish larvae. Due to air-sea ventilation of dimethylsulfide (DMS), atmospheric sulfur compounds depend on the net production of DMS in the water column, and UV radiation photolysis of DMS represents an important removal process (Deal et al., 2005). Thus, since sources of atmospheric sulfur compounds are involved in cloud formation, the abundance of algae may indirectly affect atmospheric transmission, thereby linking atmospheric radiative transfer with ocean biology.

Major gaps in our present knowledge maybe illustrated by the following questions:

1. Which scattering and absorption agents of biogenic and non-biogenic origin are responsible for the scattering and absorption of UV radiation and visible light in the water column?
2. To what extent are current radiative transfer models able to predict the spectral UV radiation and visible light as a function of depth in the water column?
3. To what extent are current radiative transfer models able to predict the UV and visible spectral radiances emanating from the water column (the so-called water-leaving radiance), and transmitted to the top of the atmosphere?
4. What measurements are needed to test models of radiative transfer in an atmosphere-ocean system that includes an aerosol-loaded or cloudy atmosphere overlying open oceanic water or bodies of turbid water, such as lakes, rivers, and estuarine coastal waters?
5. What light measurements and modeling activities are required to validate remote sensing efforts aimed at characterizing biological productivity of water in the world's oceans as well as water quality of lakes, rivers, and estuarine coastal waters?
6. What is the minimum and what is the ideal number of spectral elements that need to be recorded by remote sensing instruments in order to accurately retrieve water properties in different water regimes?

Questions 1 and 2 are important because they are relevant to our basic understanding of the main drivers of biology in aquatic systems: the UV radiation and visible light fields. Lack of, or an incomplete understanding of, how UV radiation and visible light fields vary in an aquatic ecosystem, and how they relate to scattering and absorption properties of the water constituents, is a major obstacle to the prediction of how an aquatic ecosystem will function in a changing environment, e.g., how it will respond to expected changes, including global warming and ozone depletion. Attempts to assess the impact of UV radiation penetration on aquatic ecosystems have been made by several investigators as discussed by Häder et al. (1998), and efforts are currently underway to address

the effect of stratospheric ozone variations on underwater UV irradiances on a global scale (Vasilkov et al., 2001) by making use of data from the Total Ozone Mapping Spectrometer and the Sea-viewing Wide Field-of-view Sensor (SeaWiFS).

Questions 3 − 6 must be addressed if we are to use the radiation reflected from the atmosphere-ocean system to retrieve information about biological productivity and water quality. The spectral dependence of the water-leaving radiance (i.e., the ocean color) carries information about the optical properties of the water column. If we know how these wavelength (color) dependent optical properties depend on the water constituents, we are in a position to retrieve important information about atmospheric parameters (e.g., aerosol type and optical depth) and marine parameters (e.g., concentrations of chlorophyll, dissolved and particulate organic matter, and suspended inorganic material) from measured water-leaving radiances (Stamnes et al., 2003; Li et al., 2008). Soil material, as well as man-made chemicals and agricultural fertilizing agents, are frequently transported into coastal and estuarine waters by rivers. Knowledge of how the optical properties of water are affected by such river discharges could be used to determine water quality if reliable models were available that related optical properties to water constituents of natural and anthropogenic origin. However, the retrieval of water-leaving radiances from measurements obtained with instruments deployed on earth-orbiting satellites requires accurate removal of the atmospheric component of measured radiances. This task is very difficult because the atmospheric aerosol optical properties vary rapidly, both spatially and temporally. The difficulty is compounded by the fact that 90% of the signal measured by downward-looking sensors in space comes from the atmosphere (Gordon, 1997), which means that accurate removal of the highly varying atmospheric contribution to a measured radiance becomes crucially important.

We start by providing a brief review of how UV radiation and visible light propagate throughout an atmosphere-ocean system. Then we give a few examples to illustrate possible applications of the theory: (1) comparing the results of two different radiative transfer models; (2) comparing measured and modeled radiation fields in sea ice; (3) discussing how multiple scattering in sea ice gives rise to radiation trapping; and (4) discussing how a polar ozone depletion might influence the primary production in icy polar waters.

9.2 Radiative Transfer Modeling

9.2.1 Sun-Earth Geometry

Because the earth moves around the sun in an elliptical orbit, the earth-sun distance, R, varies throughout the year, by about 3.4% from its minimum value on about

January 3 to its maximum value on about July 3. Thus, the variation in R^2 and therefore, in the extraterrestrial solar irradiance, is about 6.9%, which implies that the radiation incident at the top of the atmosphere is almost 7% larger in January (Southern hemisphere) than in July (Northern hemisphere).

The illumination of the earth's surface depends on the solar zenith angle, θ_0, which is the angle between the local zenith and the direction of the center of the solar disk. The solar zenith angle depends on the time of the day, the time of the year, and geographic location.

9.2.2 Spectrum of Solar Radiation

Figure 9.1 shows the incident UV, visible, and near-infrared parts of the spectral solar irradiance (wavelengths shorter than 1,000 nm) measured on board an earth-orbiting satellite (Rottman et al., 1993). Spectra of an ideal blackbody at several temperatures are also shown in Fig. 9.1. Given the requirement that the total solar energy emitted be the same as that emitted by a blackbody, one finds that the sun's effective temperature is 5,778 K. If the radiating layers of the sun had the same temperature at all distances from its center, the solar spectrum would

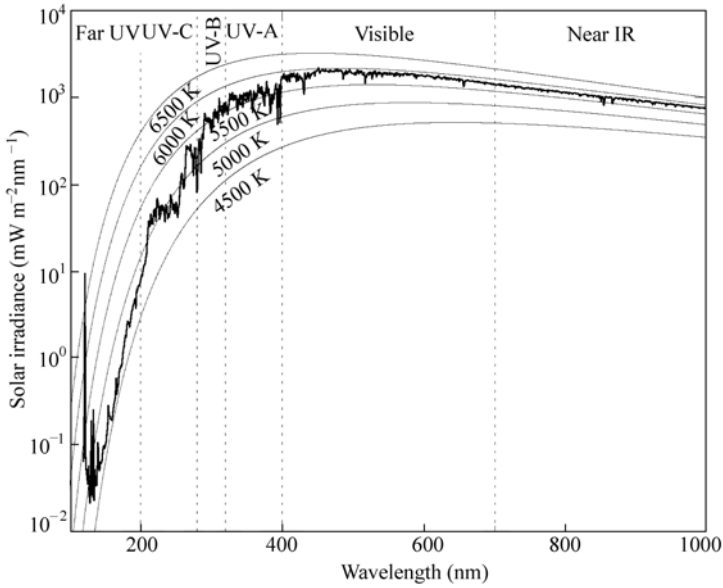

Figure 9.1 Extraterrestrial solar irradiance. The UV spectrum between 119 nm and 420 nm was measured by the SOLSTICE (SOLar STellar Irradiance Comparison Experiment) instrument on the Upper Atmosphere Research Satellite (UARS) (Rottman et al., 1993). The smooth curves are calculated blackbody spectra for several temperatures (adapted from Thomas and Stamnes, 1999)

match one of the theoretical blackbody curves exactly. Thus, the deviations between the measured solar irradiance in Fig. 9.1 and one of the blackbody curves are the result of emission from a non-isothermal solar atmosphere. Most of the solar emission arises within the photosphere where the sun's visible optical depth reaches unity. The fine structure in Fig. 9.1 is due to Fraunhofer absorption by gases in the cooler (more distant) portions of the photosphere. The effective radiating temperature falls to values as low as 4,500 K at wavelengths between 125 nm and 380 nm. Additionally, the UV irradiance is noticeably dependent upon the solar cycle, being more intense at high solar activity than at low solar activity. Thus, the solar illumination varies on diurnal, seasonal as well as the 11-year solar cycle time scales (Thomas and Stamnes, 1999). The 11-year solar cycle is associated with the variation in the number of sunspots.

9.2.3 Atmospheric Vertical Structure

The stratified vertical structure of the bulk properties of an atmosphere is a consequence of hydrostatic balance. For an atmosphere in a state of rest, the pressure, p, must support the weight of the fluid above it. By equating pressure forces and gravitational forces, one finds that $\mathrm{d}p = -g\rho\mathrm{d}z$ where g is the acceleration due to gravity, ρ is the air density, and dp is the differential change in pressure over the small height interval dz. Combining this equation with the ideal gas law $\rho = \bar{M}p / RT = \bar{M}n$, one finds upon integration

$$p(z) = p_0(z)\exp[-\int_{z_0}^{z} \mathrm{d}z' / H(z')] \tag{9.1}$$

where $\bar{M}$ is the mean molecular weight, T the temperature, R the gas constant, and $H = \mathrm{RT}/\bar{\mathrm{M}}\mathrm{g}$ the atmospheric scale height. The ideal gas law allows us to write similar expressions for the density, ρ, and the concentration, n. Clearly, from a knowledge of the surface pressure $p(z_0)$ and the variation of the scale height $H(z)$ with height z, the hydrostatic Eq. (9.1) allows us to determine the bulk gas properties at any height. Equation (9.1) applies to well-mixed gases, but not to short-lived species such as ozone, which is chemically created and destroyed.

The total number of air molecules in a 1 m^2 wide vertical column extending from sea level to the top of the atmosphere is 2.15×10^{29} molecules. In comparison the total column amount of ozone is about 1.0×10^{23} molecules m^{-2}. The height in millicentimeters (10^{-5} m) that the ozone gas in the atmosphere would occupy, if it were compressed to standard pressure (1,013 [hP]; 1 hP (hectoPascal) = 1 $\mathrm{N\cdot m}^{-2}$) at standard temperature (0°C), is called the Dobson unit (DU). Thus, one Dobson unit refers to a layer of ozone that would be 10 μm thick under standard temperature and pressure. The conversion is 1 DU = 2.69×10^{20} molecules m^{-2}. The 1976 US Standard Atmosphere (Anderson et al., 1987) contains about 348 DU of ozone gas.

9.2.4 Light Interaction with Absorbing and Scattering Media

The absorption coefficient $\alpha(\lambda)$, the scattering coefficient $\sigma(\lambda)$, and the scattering phase function $p(\lambda,\Theta)$, can be expressed as:

$$\alpha(\lambda) = \sum_i \alpha_i(\lambda) \tag{9.2}$$

$$\sigma(\lambda) = \sum_i \sigma_i(\lambda) \tag{9.3}$$

$$p(\lambda,\Theta) = \sum_i \frac{\sigma_i(\lambda) p_i(\lambda,\Theta)}{\sigma(\lambda)} \tag{9.4}$$

The subscript *i* is used to denote the various radiatively-active components, i.e., air molecules, aerosols, and liquid water and ice cloud particles in the atmosphere; ice crystals and impurities in the snow; brine pockets and air bubbles in the ice; pure water mixed with air bubbles, chlorophyll, inorganic particles, and yellow substance in the ocean. Here λ is the wavelength, and Θ is the scattering angle, which is related to the polar and azimuthal angles through the cosine law of spherical geometry:

$$\cos\Theta = \cos\theta\cos\theta' + \sin\theta\sin\theta'\cos(\phi - \phi')$$

Here (θ',ϕ') denotes the radiation direction prior to scattering and (θ,ϕ) is the radiation direction after scattering.

9.2.4.1 Absorption and Scattering by Atmospheric Molecules and Pure Water

Absorption by molecules in the earth's atmosphere is due to radiatively-active trace gases. For UV radiation and visible light the most important gas is ozone, but oxides of sulfur and nitrogen may (depending on location) have a significant effect on the UV radiation penetration. In the relatively pristine polar regions, we may assume that for UV radiation and visible light, ozone is the only significant absorbing gas in the atmosphere. Thus, the molecular absorption coefficient becomes:

$$\alpha_m(\lambda) = \alpha_{n,\mathrm{O_3}} n_{\mathrm{O_3}} \tag{9.5}$$

where the subscript *m* stands for molecules, and $\alpha_{n,\mathrm{O_3}}$ and $n_{\mathrm{O_3}}$ are the ozone absorption cross section and number density, respectively (Figs. 9.2(a), (b)). At wavelengths longer than 310 nm, the ozone absorption is due to the Huggins bands, whereas the spectrally-broad but weak absorption between 450 and 700 nm is due to the Chappuis bands (Fig. 9.2(a)).

Scattering by molecules in the atmosphere is proportional to the gas density. Thus, the scattering coefficient due to scattering by air molecules is:

$$\sigma_m(\lambda) = \sigma_{n,\mathrm{Ray}}(\lambda) n_m \tag{9.6}$$

where $\sigma_{n,\mathrm{Ray}}(\lambda) \sim \lambda^{-4}$ is the Rayleigh scattering cross section, and n_m is the total air number density (Fig. 9.2(b)).

Absorption by pure water results from mutual interactions between the intermolecular forces. Calculation of absorption cross sections from first principles is very difficult. Thus, laboratory and *in situ* measurements (Pegau et al., 1995; Pope and Fry, 1997) become essential for establishing the absorption coefficient $\alpha_{n,w}(\lambda)$ for pure water (Fig. 9.2(c)).

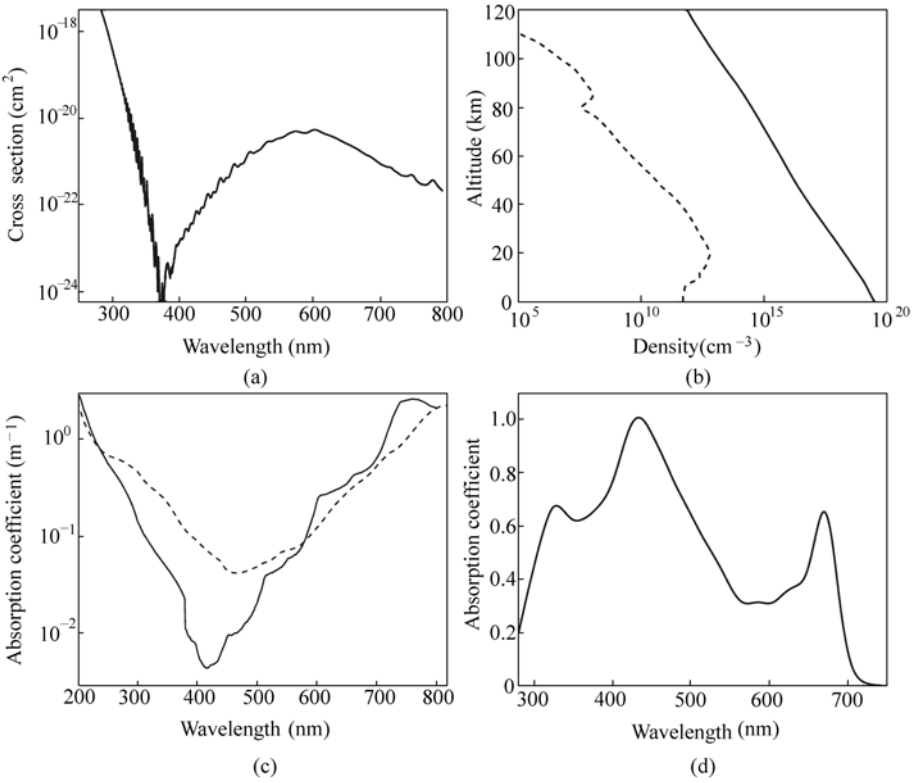

Figure 9.2 (a) Absorption cross section of ozone; (b) number density of atmospheric ozone (dashed line) and total air number density (solid line); (c) absorption spectrum for pure ice (dashed line), and for pure water (solid line; (d) chlorophyll-specific absorption spectrum normalized at 440 nm

Scattering in pure water is due to clusters of molecules and ions, much smaller than the wavelength of light, and from an optical point of view, the clusters are uncorrelated (Thomas and Stamnes, 1999). Thus, the wavelength dependence of the scattering cross section for pure water is $\sigma_{n,w}(\lambda) \sim \lambda^{-4.32}$, similar to the Rayleigh scattering cross section for molecules in the atmosphere. The scattering coefficient for pure water can be approximated by (Morel, 1974):

$$\sigma_w(\lambda) = \left(\frac{129}{\lambda}\right)^{4.32} \qquad \lambda \text{ in [nm].}$$

The phase function for scattering by atmospheric molecules or by pure water is given by:

$$p_w(\Theta) = \frac{3}{(3+x)} \cdot (1 + x\cos^2\Theta)$$

For scattering by air molecules (Rayleigh scattering), the parameter x is set equal to 1, while for scattering by pure water, $x = 0.835$. The latter value of x can be attributed to the anisotropy of the water molecule (Mobley, 1994; Morel and Gentili, 1991).

9.2.4.2 Absorption and Scattering by Particles

In addition to molecules, suspended particulate matter in the atmosphere and ocean has a significant impact on the radiative transfer. This particulate matter consists of aerosols (dust, sulfate particles, soot, smoke particles, cloud water droplets, raindrops, ice crystals, etc.) in the atmosphere, snow grains, air bubbles and brine pockets in ice, and hydrosols (suspended particles of organic and inorganic origin) in the water. Thus, to describe radiative transfer in a medium such as the coupled atmosphere-snow-ice-ocean (CASIO) system, we may think of it as being composed of randomly distributed, radiatively-active 'particles' that absorb and scatter radiation.

We assume that the optical properties of particles (i.e., aerosols, cloud particles, snow grains, brine pockets, etc.) can be approximated by those of spheres. Then, the absorption and scattering coefficients and the scattering phase function can be written as:

$$\alpha_p(\lambda) = \int_{r_{\min}}^{r_{\max}} \pi r^2 Q_\alpha(r) n(r) \mathrm{d}r \tag{9.7}$$

$$\sigma_p(\lambda) = \int_{r_{\min}}^{r_{\max}} \pi r^2 Q_\sigma(r) n(r) \mathrm{d}r \tag{9.8}$$

$$p_p(\lambda,\Theta) = \frac{\int_{r_{\min}}^{r_{\max}} p_p(\lambda,\Theta,r) n(r) \mathrm{d}r}{\int_{r_{\min}}^{r_{\max}} n(r) \mathrm{d}r} \tag{9.9}$$

where $Q_\alpha(r)$ or $Q_\sigma(r)$ is defined as the ratio of the absorption or scattering cross section for a spherical particle of radius r to the geometrical cross section πr^2, $n(r)$ is the particle size distribution, and r is the radius of each individual particle. For a specific value of r, we can compute $Q_\alpha(r)$, $Q_\sigma(r)$, and $p_p(\lambda,\Theta,r)$ using Lorenz-Mie theory, but evaluation of Eqs. (9.7) – (9.9) requires knowledge of the

particle size distribution $n(r)$, which is usually unknown.

Hamre et al. (2004) showed that Eqs. (9.7) – (9.9) can be considerably simplified by making the following assumptions:

- The particle distribution is characterized by an effective radius $r_e = \int_{r_{\min}}^{r_{\max}} n(r) r^3 \mathrm{d}r \Big/ \int_{r_{\min}}^{r_{\max}} n(r) r^2 \mathrm{d}r$, which obviates the need for an integration over r.
- The particles are weakly absorbing, so that $Q_\alpha(r) \approx \frac{16\pi r m_{i,p}}{3\lambda} \cdot \frac{1}{m_{\mathrm{rel}}} \cdot [m_{\mathrm{rel}}^3 - (m_{\mathrm{rel}}^2 - 1)^{3/2}]$, where $m_{i,p}$ is the imaginary part of the refractive index of the particle, λ is the wavelength in vacuum, and $m_{\mathrm{rel}} = m_{r,p} / m_{r,\mathrm{med}}$ is the ratio of the real part of the refractive index of the particle ($m_{r,p}$) to that of the surrounding medium ($m_{r,\mathrm{med}}$).
- The particles are large compared to the wavelength ($2\pi r / \lambda >> 1$), which implies $Q_\sigma(r) = 2$.
- The scattering phase function can be represented by the one parameter Henyey-Greenstein phase function, which depends only on the asymmetry factor $g \equiv \langle \cos\Theta \rangle = \frac{1}{2} \int_{-1}^{1} p(\Theta) \cos\Theta \mathrm{d}(\cos\Theta)$.

With these assumptions, Eqs. (9.7) – (9.9) become:

$$\alpha_p(\lambda) = \alpha(\lambda) \cdot \frac{1}{m_{\mathrm{rel}}} \cdot \left[1 - (m_{\mathrm{rel}}^2 - 1)^{3/2}\right] f_V \tag{9.10}$$

$$\sigma_p(\lambda) = \frac{3}{2} \cdot \frac{f_V}{r_e} \tag{9.11}$$

$$p_p(\lambda, \Theta) = \frac{1 - g^2}{(1 + g^2 - 2g\cos\Theta)^{3/2}} \tag{9.12}$$

where $\alpha(\lambda)$ is the absorption coefficient for the material of which the particle is composed, and $f_V = \frac{4}{3}\pi r^3 n_e$, where n_e is the number of particles per unit volume with radius r_e.

9.2.4.3 Optical Properties of the Ocean

To represent the optical properties of the water beneath the ice, we may use the model of Morel (1991), updated by Morel and Maritorena (2001), according to which the absorption and scattering coefficients and the scattering phase function are given by:

$$\alpha(\lambda) = \alpha_w(\lambda) + \alpha_C(\lambda) + \alpha_Y(\lambda) \tag{9.13}$$

$$\sigma(\lambda) = \sigma_w(\lambda) + \sigma_C(\lambda) \tag{9.14}$$

$$p(\lambda,\Theta) = \frac{\sigma_w(\lambda)p_w(\lambda,\Theta) + \sigma_C(\lambda)p_C(\lambda,\Theta)}{\sigma(\lambda)} \tag{9.15}$$

where the subscript *w* denotes pure water, the subscript *C* denotes chlorophyll-*a* related absorption and scattering, and the subscript *Y* stands for yellow substance. The absorption coefficient for pure water was discussed above (see Fig. 9.2(c)), and

$$\alpha_C(\lambda) = 0.064 A_C(\lambda) C^{0.65}$$

where $A_C(\lambda)$ is the normalized absorption spectrum for the chlorophyll-*a* related absorption displayed in Fig. 9.2(d), and $C(\mathrm{mg \cdot m^{-3}})$ is the chlorophyll-*a* concentration. The absorption by yellow substance is expressed as:

$$\alpha_Y(\lambda) = \alpha_Y(440)\exp[-0.014(\lambda - 440)]$$

where $\alpha_Y(440) = 0.2[\alpha_w(440) + 0.064 A_C(440) C^{0.65}]$, and the chlorophyll-*a* related scattering coefficient is given by:

$$\sigma_C(\lambda) = 0.3\left(\frac{550}{\lambda}\right) C^{0.62}$$

Scattering by pure water was discussed in Section 9.2.4.1.

9.2.4.4 Definitions of Irradiance and Radiance

The spectral net irradiance F_ν is defined as the net energy d^3E crossing a surface element $\mathrm{d}A$ (with unit normal $\hat{n}$) per unit time and per unit frequency (Thomas and Stamnes, 1999):

$$F_\nu = \frac{\mathrm{d}^3E}{\mathrm{d}A\mathrm{d}t\mathrm{d}\nu} \qquad [\mathrm{W \cdot m^{-2} \cdot Hz^{-1}}].$$

Since the irradiance is positive if the energy flow is into the hemisphere centered on the direction $\hat{n}$ and negative if the flow is into the opposite hemisphere, we may define spectral hemispherical irradiances $F_\nu^+ = \mathrm{d}^3E^+ / \mathrm{d}A\mathrm{d}t\mathrm{d}\nu$ and $F_\nu^- = \mathrm{d}^3E^- / \mathrm{d}A\mathrm{d}t\mathrm{d}\nu$. Thus, the spectral net irradiance becomes $F_\nu = F_\nu^+ - F_\nu^-$, and integration over all frequencies yields the net irradiance $F = \int_0^\infty \mathrm{d}\nu F_\nu$ $[\mathrm{W \cdot m^{-2}}]$.

Consider any small subset of the energy d^4E that flows within a solid angle $\mathrm{d}\omega$ around the direction $\hat{\Omega}$ in the time interval $\mathrm{d}t$ and within the frequency range $\mathrm{d}\nu$. If this subset of radiation has passed through a surface element $\mathrm{d}A$ (with unit

normal $\hat{n}$), then the energy per unit area per unit solid angle, per unit frequency, and per unit time, defines the spectral radiance I_ν:

$$I_\nu = \frac{\mathrm{d}^4 E}{\cos\theta \mathrm{d}A \mathrm{d}t \mathrm{d}\omega \mathrm{d}\nu} \qquad [\mathrm{W \cdot m^{-2} \cdot sr^{-1} \cdot Hz^{-1}}].$$

Here θ is the angle between the surface normal $\hat{n}$ and the direction of propagation $\hat{\Omega}$. It is clear from these definitions that $F_\nu^+ = \int_+ \mathrm{d}\omega \cos\theta I_\nu$ and $F_\nu^- = -\int_- \mathrm{d}\omega \cos\theta I_\nu$. Thus, the spectral net irradiance can be expressed as:

$$F_\nu = F_\nu^+ - F_\nu^- = \int_{4\pi} \mathrm{d}\omega \cos\theta I_\nu .$$

Finally, we define the mean intensity as: $\overline{I} = (1/4\pi)\int_{4\pi} \mathrm{d}\omega I_\nu$, which is simply the radiance averaged over the sphere.

9.2.4.5 Absorption, Scattering, and Extinction by Molecules and Particles

A beam of light incident on a thin layer with thickness ds of radiatively-active matter (gases and/or particles) is attenuated so that the differential loss in radiance is proportional to the incident light: $\mathrm{d}I_\nu = -k(\nu,s) I_\nu \mathrm{d}s$, where $k(\nu,s)$ is called the extinction or attenuation coefficient. Integration yields

$$I_\nu(s,\hat{\Omega}) = I_\nu(0,\hat{\Omega}) \exp[-\tau_s(\nu)], \tag{9.16}$$

where $\hat{\Omega}$ denotes the propagation direction of the beam. The dimensionless extinction (or attenuation) optical path (or opacity) along the path s is given by $\tau_s(\nu) \equiv \int_0^s \mathrm{d}s'\, k(\nu,s')$. Attenuation of a light beam can be caused by either absorption or scattering. The extinction (or attenuation) optical path of a mixture of scattering/absorbing molecules and particles is defined as the sum of the scattering and absorption optical paths, $\tau_s(\nu) = \tau_{sc}(\nu) + \tau_a(\nu)$, where $\tau_{sc}(\nu) = \sum_i \int_0^s \mathrm{d}s' \sigma_i(\nu,s')$ and $\tau_a(\nu) = \sum_i \int_0^s \mathrm{d}s' \alpha_i(\nu,s')$. The sum is over all optically active species (each denoted by the subscript i), and $\sigma_i(\nu,s)$ and $\alpha_i(\nu,s)$ [$\mathrm{m^{-1}}$] are the scattering and absorption coefficients, and $k_i(\nu,s) = \alpha_i(\nu,s) + \sigma_i(\nu,s)$ is the extinction or attenuation coefficient. These are defined as $\sigma_i(\nu,s) = \sigma_{n,i}(\nu) n_i(s)$ and $\alpha_i(\nu,s) = \alpha_{n,i}(\nu) n_i(s)$, where n_i [$\mathrm{m^{-3}}$] is the concentration and $\alpha_{n,i}(\nu)$ and $\sigma_{n,i}(\nu)$ [$\mathrm{m^2}$] are the absorption and scattering cross sections of the ith optically active species (molecule or particle).

9.2.5 Equation of Radiative Transfer

If we are interested primarily in energy transfer, rather than the directional dependence of the radiation, it is sufficient to work with the azimuthally-averaged radiance $I_\nu(z,u)$, where z denotes the level in the medium (height in the atmosphere or depth in the ocean), and $u=\cos\theta$, θ being the polar angle. It is convenient to split the radiation field into two parts: (1) the *direct* solar beam, which is exponentially attenuated upon passage through the atmosphere and ocean, and (2) the *diffuse* or scattered radiation.

According to Eq. (9.16), the penetration of the direct solar beam through the atmosphere may be written as $I_{\text{sol}}(s,\hat{\Omega}) = F^s\ \delta(\hat{\Omega}-\hat{\Omega}_0)\,\mathrm{e}^{-\tau_s(\nu)}$. Here $\hat{\Omega}_0=(\theta_0,\phi_0)$ is a unit vector in the direction of the incident solar beam, where $\mu_0=\cos\theta_0$, and θ_0 is the solar zenith angle as illustrated in Fig. 9.3. F^s is the solar irradiance (normal to the solar beam direction $\hat{\Omega}_0$) incident at the top of the atmosphere. In plane-parallel geometry, the vertical optical depth is defined in terms of the optical path $\tau_s(\nu)$ as follows:

$$\tau(\nu,z)\equiv\tau_s(\nu)/\mu_0\equiv\sum_i\int_z^\infty \mathrm{d}z'\,k^i(\nu,z')$$

or

$$\mathrm{d}\tau(\nu,z)=-k(\nu,z)\mathrm{d}z=-\sum_i[\alpha_{n,i}(z)+\sigma_{n,i}(z)]n_i(z)\mathrm{d}z$$

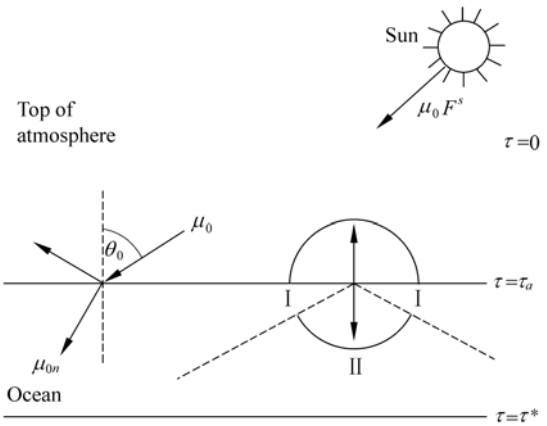

Figure 9.3 Schematic illustration of two adjacent media with a flat interface, such as the atmosphere overlying a calm ocean. Because the real part of the refractive index (m_r) of the atmosphere ($m_{\text{atm},r}\approx 1$) is different from that of the ocean ($m_{\text{ocn},r}\approx 1.33$), radiation distributed over $2\pi\,sr$ in the atmosphere will be confined to a cone less than $2\pi\,sr$ in the ocean (region Ⅱ). Radiation in the ocean within region Ⅰ will be totally reflected when striking the interface from below (Thomas and Stamnes, 1999)

so that for a plane-parallel medium the direct component becomes:

$$I_{\text{sol}}(\tau,u,\phi) = F^s \delta(u-\mu_0)\delta(\phi-\phi_0)\,\mathrm{e}^{-\tau/\mu_0} \tag{9.17}$$

Here $u=\cos\theta$, θ is the polar angle of the observation direction, $\mu=|u|$, and ϕ denotes the azimuth angle of the observation direction.

In a stratified medium, the optical properties vary only in the vertical direction, and the transfer of diffuse radiation through such a medium is described by:

$$u\frac{\mathrm{d}I(z,u)}{\mathrm{d}z} = -k(z)I(z,u) + \sigma(z)\frac{1}{2}\int_{-1}^{1}\mathrm{d}u'\; p(z,u',u)I(z,u') + S^*(z,u) \tag{9.18}$$

where $I(z,u)$ is the azimuthally-averaged diffuse radiance. The term on the left side in Eq. (9.18) is the change in the diffuse radiance $I(z,u)$ along a slant path dz/u. The first term on the right side is the loss of radiation out of the beam due to extinction, and the second term is the gain due to multiple scattering. The third term, $S^*(z,u)$ defined below, is the solar pseudo-source, proportional to the attenuated solar beam, which 'drives' the diffuse radiation. Using the non-dimensional optical depth, $\mathrm{d}\tau(z) = -k(z)\mathrm{d}z$ as the independent variable, we may rewrite Eq. (9.18) as follows:

$$u\frac{\mathrm{d}I(\tau,u)}{\mathrm{d}\tau} = I(\tau,u) - \frac{a(\tau)}{2}\int_{-1}^{1}\mathrm{d}u'\; p(\tau,u',u)\,I(\tau,u') - S^*(\tau,u) \tag{9.19}$$

where the single-scattering albedo is defined as $a(\tau(z)) \equiv \sigma(z)/k(z)$.

9.2.6 Surface Reflection and Transmission

It is necessary to consider two strata for a coupled atmosphere-ocean system; one for the atmosphere with real part of the refractive index $m_{\text{atm},r}$ and another for the ocean with real part of the refractive index $m_{\text{ocn},r}$. The basic radiance, defined as I/m_r^2, where m_r is the real part of the refractive index, is a conserved quantity. Thus, if we neglect reflection losses, the basic radiance will be constant across the interface between the two strata. Assuming for simplicity that the interface is flat and smooth (a calm ocean), then the radiance must satisfy Snell's law and Fresnel's equations. As illustrated in Fig. 9.3, the downward radiation distributed over $2\pi sr$ in the atmosphere will be restricted to a cone less than $2\pi sr$ (referred to as region Ⅱ in Fig. 9.3) after being refracted across the interface into the ocean. Outside the refractive region in the ocean, i.e., in the total reflection region (referred to as region Ⅰ in Fig. 9.3), the radiation is due to in-water multiple scattering. The demarcation between the refractive region and the total reflection region in the ocean is given by the critical angle θ_c given by

$\mu_c \equiv \cos\theta_c = \sqrt{1-1/m_{\text{rel}}^2}$, where $m_{\text{rel}} = m_{\text{ocn},r} / m_{\text{atm},r}$ is the real part of the refractive index in the ocean relative to that in the atmosphere.

Because the radiation field in the ocean is driven by solar radiation passing through the atmosphere-water interface, Eq. (9.19) applies also in the ocean, but the solar pseudo-sources are different in the two media. In the atmosphere we have:

$$S^*_{\text{atm}}(\tau,u) = \frac{a(\tau)}{4\pi} p(\tau,-\mu_0,u)\, \mathrm{e}^{-\tau/\mu_0} + \frac{a(\tau)}{4\pi} \rho_s(-\mu_0;m_{\text{rel}})\, p(\tau,\mu_0,u)\, \mathrm{e}^{-(2\tau_a-\tau)/\mu_0}$$

Here the first term is the usual solar beam pseudo-source, and the second term is due to the reflection occurring at the interface, which is proportional to $\rho_s(-\mu_0;m_{\text{rel}})$, the specular reflectance. The pseudo-source in the ocean is just the attenuated solar beam refracted through the interface:

$$S^*_{\text{ocn}}(\tau,u) = \frac{a(\tau)}{4\pi} \cdot \frac{\mu_0}{\mu_{0m}} T_b(-\mu_0;m_{\text{rel}})\, p(\tau,-\mu_{0m},u)\, \mathrm{e}^{-\tau_a/\mu_0}\, \mathrm{e}^{-(\tau-\tau_a)/\mu_{0m}}$$

Here $T_b(-\mu_0;m_{\text{rel}})$ is the beam transmittance through the interface, and μ_{0m} is the cosine of the solar zenith angle in the ocean, which is related to μ_0 by Snell's law $\mu_{0m} \equiv \mu_{0m}(\mu_0,m_{\text{rel}}) = \sqrt{1-(1-\mu_0^2)/m_{\text{rel}}^2}$. With the use of the appropriate pseudo-sources for the atmosphere [$S^*_{\text{atm}}(\tau,u)$] and ocean [$S^*_{\text{ocn}}(\tau,u)$], Eq. (9.19) can now be solved subject to boundary conditions at the top of the atmosphere and the bottom of the ocean. However, we must also properly account for the reflection from and transmission through the atmosphere-ocean interface by requiring that Fresnel's equations are satisfied.

9.2.7 Radiative Transfer in a Coupled Atmosphere-Snow-Ice-Ocean (CASIO) System

Solar irradiance levels play a key role for energy exchange and primary production in marine polar environments. Because the ocean is typically covered by sea ice and snow for several months of the year, theoretical and experimental knowledge of radiation levels at various depths in the snow, ice, and ocean is essential. The photosynthetically active radiation (PAR, 400 nm$< \lambda <$700 nm) drives the pelagic primary production in general, and the amount of PAR reaching the bottom of the sea ice is of crucial importance for the growth of ice algae, which accounts for between 5% and 30% of the total plankton production in the polar regions (Legendre et al., 1992; Wheeler et al., 1996). The wavelength dependence of UV radiation ($\lambda <$400 nm) is required to assess potential damage and inhibition of primary production induced by UV radiation (Neal et al., 1998). Finally, the amount of radiation that penetrates the snow and ice determines the rate of energy

absorption, melting of sea ice, and warming of the upper ocean (Perovich and Maykut, 1996; Zeebe et al., 1996).

Here we provide a brief description of the CASIO Discrete-Ordinate Radiative Transfer (CASIO-DISORT) model, which treats transfer of solar radiation in the CASIO system based on the theory provided above and its implementation by use of the discrete-ordinate method. Note that in the absence of sea ice, the CASIO system defaults to the CAO (coupled atmosphere-ocean) system.

In summary, the CASIO-DISORT method works as follows:

(1) The atmosphere and the ice-ocean media are treated as two adjacent slabs separated by an interface across which the real part of the refractive index changes from $m_{\mathrm{atm},r} = 1$ in the atmosphere (including a possible snow layer at the bottom, i.e., on top of the ice) to $m_{\mathrm{ocn},r} = 1.31$ (1.33 in the absence of ice) in the ice-ocean medium.

(2) Each of the two slabs is divided into a sufficient number of horizontal layers to adequately resolve vertical variations in their inherent optical properties.

(3) The reflection and transmission through the interface between the atmosphere and the ice-ocean are computed by Fresnel's equations, and the reflection and refraction of a beam at the interface follow the reflection law and Snell's law, respectively.

(4) The radiative transfer equation is solved separately for each layer in the atmosphere and in the ice-ocean using the discrete-ordinate method.

(5) The solution is completed by applying boundary conditions at the top of the atmosphere and the bottom of the ocean, as well as appropriate radiance continuity conditions at each layer interface in the atmosphere, in the ice-ocean media, and at the atmosphere-ice-ocean interface (where Fresnel's equations apply).

9.3 Sample Applications of the Theory

9.3.1 Comparison of Modeled Irradiances in CAO Systems

Gjerstad et al. (2003) undertook a study aimed at comparing two distinctly different methods of solving the radiative transfer equation for coupled atmosphere-ocean systems. One of these methods was the deterministic discrete-ordinate method (Stamnes et al., 1988; 2000), extended to apply to two adjacent slabs with different indices of refraction, such as a coupled atmosphere-ocean (CAO) system (Jin and Stamnes, 1994). The other method was the Monte Carlo (MC) approach, in which the trajectories of individual photons were simulated (Collins et al., 1972; Lenoble, 1985).

Mobley et al. (1993) compared underwater light fields computed by several different methods, including MC methods and the discrete-ordinate method, and showed that different methods give similar results for a limited set of test cases. However, the models included the atmosphere in different ways, which led to a spread in the downward irradiance of 18% just above the water surface and throughout the underwater column. Also, no comparisons of atmospheric irradiances were made. To remedy this shortcoming Gjerstad et al. (2003) performed a detailed quantitative comparison of irradiances simulated with a Monte Carlo method with those computed with a CAO-DISORT model (Jin and Stamnes, 1994; Thomas and Stamnes, 1999).

The CAO-MC and the CAO-DISORT models used by Gjerstad et al. (2003) had precisely the same physical basis, including coupling between the atmosphere and the ocean, and precisely the same atmospheric and ocean input parameters. Computed results for direct and diffuse upward and downward irradiances are shown in Fig. 9.4. The percentage deviation is less than 0.5% for downward irradiances, and less than 1% for upward irradiances. The CAO-MC code has an

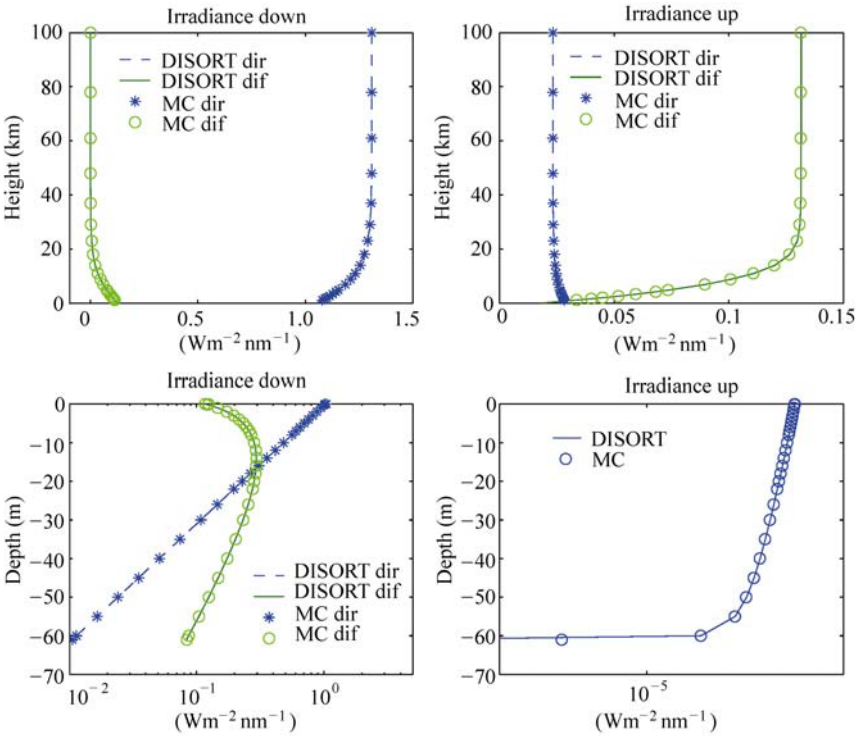

Figure 9.4 Comparison of irradiances computed by a CAO-DISORT code (solid and dashed curves) and a CAO-MC code (circles and asterisks). For details, see Gjerstad et al. (2003)

advantage over the CAO-DISORT (Jin and Stamnes, 1994) code in that it can handle surface waves, but the CAO-DISORT code is computationally much faster. Finally, it should be noted that Jin et al. (2006) recently extended the CAO-DISORT code to include the effects of surface waves.

9.3.2 Measured and Modeled Radiation Fields in Sea Ice

The theory described above was applied to analyze a comprehensive set of measurements taken in Kongsfjorden, Svalbard (Gerland et al., 1999; Hamre et al., 2004). Physical and structural properties (snow and ice thickness, density, *in situ* temperature, and salinity profiles) were measured in addition to irradiances above the surface and under the ice. On the basis of measured snow grain sizes, snow depth, ice temperature, and ice salinity, Hamre et al. (2004) computed the transmittance of first-year sea ice with and without snow cover. These computations were done with a CASIO-DISORT code, and the bubble sizes and the snow grain sizes were estimated by assuming that the absorption by impurities can be neglected at near-infrared wavelengths. Also, it was assumed that the volume fractions of air bubbles and brine pockets (f_V^{bu} and f_V^{br}) could be determined from the salinity, bulk ice density, and temperature (Cox and Weeks, 1983; Jin et al., 1994). The results of this study may be summarized as follows:

- a best fit between measured and computed transmittances was obtained with snow grains that were only 5% larger than the smallest observed values;
- the shape of the impurity absorption spectrum resulting from forcing agreement between modeled and measured transmittances resembled that of ice algae;
- a 2.5 cm-thick layer of snow had the same transmittance for visible light and UV radiation as a 61 cm-thick ice layer;
- UV radiation is removed more efficiently than visible light for snow depths greater than 3 cm − 4 cm implying that algae growing under snow cover may be protected from harmful UV radiation, yet receives sufficient visible light for photosynthesis;
- the CASIO-DISORT model is a useful tool for computing energy deposition in the snow, ice, and ocean, and can be used to investigate the influence of changes in environmental conditions, such as ozone amount, snow thickness, and cloud cover on UV radiation and visible light, and hence, on the aquatic biology in polar regions.

9.3.3 Radiation Trapping in Sea Ice

Comparisons of radiative transfer models used to compute irradiances and radiances in atmosphere-ocean systems have shown that they yield similar results

for identical input, and have clearly demonstrated the influence of the atmosphere/snow-sea ice/ocean interface on the transport of energy across it (Mobley et al., 1993; Gjerstad et al., 2003). Nevertheless, little attention has been paid to the enhanced downward irradiance (EDI) across the atmosphere-sea ice interface due to trapping of light caused by multiple scattering in the sea ice. The EDI is defined as:

$$\Delta F_{\mathrm{d}}(\lambda) \equiv F_{\mathrm{d}}(0^{-},\lambda) - F_{\mathrm{d}}(0^{+},\lambda) \tag{9.20}$$

where $F_{\mathrm{d}}(0^{-},\lambda)$ is the downward irradiance just *below* the interface, and $F_{\mathrm{d}}(0^{+},\lambda)$ is the downward irradiance just *above* the interface. By definition, if the irradiance difference across the interface is positive ($\Delta F_{\mathrm{d}}(\lambda) > 0$), there is an EDI effect across the interface; otherwise, there is no EDI effect.

The irradiance incident on the atmosphere-sea ice interface consists of two components:

$$F_{\mathrm{d}}(0^{+},\lambda) = F_{\mathrm{sol}}(0^{+},\lambda) + F_{\mathrm{diff}}(0^{+},\lambda) \tag{9.21}$$

where $F_{\mathrm{sol}}(0^{+},\lambda)$ is the direct solar beam irradiance and $F_{\mathrm{diff}}(0^{+},\lambda)$ is the downward irradiance due to diffuse skylight. Similarly, the downward irradiance just below the interface consists of three components:

$$F_{\mathrm{d}}(0^{-},\lambda) = F_{\mathrm{trans}}(0^{-},\lambda) + F_{\mathrm{pref}}(0^{-},\lambda) + F_{\mathrm{tref}}(0^{-},\lambda). \tag{9.22}$$

Here $F_{\mathrm{trans}}(0^{-},\lambda) = F_{\mathrm{sol,\,tr}}(0^{+},\lambda) + F_{\mathrm{diff,\,tr}}(0^{+},\lambda)$ is the sum of two downward irradiance components from the atmosphere that are transmitted through the interface, $F_{\mathrm{pref}}(0^{-},\lambda)$ is the downward irradiance due to the upward radiation in the sea ice with directions inside the refraction cone that is partially reflected downwards by the interface, and $F_{\mathrm{tref}}(0^{-},\lambda)$ is the downward irradiance due to the upward radiation in the sea ice with directions outside the refraction cone that is totally reflected downwards by the interface.

Using a radiative transfer model similar to the CASIO-DISORT model described above, Jiang et al. (2005) simulated the EDI effect. Table 9.1 shows all components of the computed downward irradiance just above and just below the atmosphere-sea ice interface for a solar elevation of 30° and for a wavelength of 550 nm under clear sky conditions. The incident downward solar irradiance is 4.21 μ ein $\mathrm{m^{-2}\ s^{-1}\ nm^{-1}}$ (0.92 W $\mathrm{m^{-2}\ nm^{-1}}$). We note that $F_{\mathrm{tref}}(0^{-},\lambda)$ is the main source of the EDI effect. Thus, the EDI effect is primarily due to radiation that is totally reflected by the interface. The dominance of scattering in the ice compared to absorption is the cause of the EDI effect. The biogeophysical significance of the EDI is that the mean intensity just below the interface will be enhanced, and so will the energy available for photolysis and melting of the sea ice.

The third column in Table 9.1 demonstrates that without a jump in the index of refraction, there is no EDI effect ($\Delta F_{\mathrm{d}}(\lambda) = 0$), and the fourth column demonstrates

that in the absence of scattering in the sea ice ($b_{ice} = 0$), there is no EDI effect. In fact, $\Delta F_d(\lambda) < 0$ when $b_{ice} = 0$, which is a consequence of energy conservation, because a fraction of the irradiance incident on the ice is (Fresnel) reflected, and no light can be backscattered from the sea ice when $b_{ice} = 0$.

Table 9.1 Comparison of downward irradiance components (in units of μ ein $m^{-2}\,s^{-1}\,nm^{-1}$) at 550 nm just above and just below the atmosphere-sea ice interface*

Component	$m_{rel} = 1.31$	$m_{rel} = 1$	$b_{ice} = 0$
$F_{sol}(0^+,550)$	2.47	2.47	2.47
$F_{diff}(0^+,550)$	1.20	1.29	1.02
$F_d(0^+,550)$	3.67	3.76	3.49
$F_{sol,tr}(0^-,550)$	2.34	2.47	2.34
$F_{tref}(0^-,550)$	1.32	0	0
$F_{diff,tr}(0^-,550)$	1.08	1.29	0.92
$F_{pref}(0^-,550)$	0.11	0	0
$F_d(0^-,550)$	4.85	3.76	3.26
$\Delta F_d(550)$	1.18	0	−0.23

* The second column shows the EDI effect, the third column shows results obtained with no jump in the index of refraction, and the fourth column shows results when the scattering in the sea ice is ignored (see text above)

9.3.4 Impact of Ozone Depletion on Primary Productivity

Several studies have suggested that a depletion of the ozone layer could lead to a reduction in the primary production of aquatic ecosystems due to an increase in UV-B radiation (Häder, 1997; Häder et al., 1998). Smith et al., (1992) estimated a 6% − 12% reduction in the primary production in the marginal ice of the Southern Ocean for a reduction in the stratospheric ozone from 300 DU − 200 DU. Other studies have indicated that an ozone depletion from 300 DU − 150 DU in Antarctica would lead to a reduction in the primary production of < 3.8% (Holm-Hansen et al., 1993b), and between 8.5% and 0.7% under clear skies (6.5% and 0.8% under cloudy skies).

Many marine organisms are sensitive to UV radiation. The extent to which these marine organisms will be able to adapt to expected increases in UV exposure is uncertain due to a sparcity of measurements. Increased levels of UV-B radiation may impact phytoplankton communities by: (1) initiating changes in cell size and taxonomic structure, (2) reducing the productivity, (3) influencing the protein content, dry weight, and pigment concentration, (4) inducing chloroplast damage, and (5) directly affecting the proteins of the photosynthetic apparatus.

To explore the potential impact of ozone depletions, one may use a simple model, in which marine photosynthesis (or primary production, ignoring respiratory losses)

is parameterized as follows (Cullen et al., 1992; Neal et al., 1998):

$$P = P_s\left(1 - \mathrm{e}^{I_p / I_s}\right)\frac{1}{1 + I^*} \tag{9.23}$$

where P_s is the maximum photosynthesis in the absence of UV radiation inhibition, and I_p is the photosynthetically utilizable radiation (PUR):

$$I_p = \int_{400}^{700} \overline{I}(\lambda) a^*(\lambda) \mathrm{d}\lambda \tag{9.24}$$

Here, $\overline{I}(\lambda)$ is the mean intensity (scalar irradiance), and $a^*(\lambda)$ the normalized algal absorption spectrum. In Eq. (9.23), I_s is the PUR saturation level, and $1/(1 + I^*)$ describes the inhibition caused by UV radiation (UVR), where I^* is given by:

$$I^* = \int_{280}^{400} \varepsilon(\lambda) \overline{I}(\lambda) \mathrm{d}\lambda \tag{9.25}$$

Here, $\varepsilon(\lambda)$ is the action spectrum for UVR-induced inhibition of photosynthesis.

The mean intensity $\overline{I}(\lambda)$ that drives and inhibits primary photosynthesis depends on several environmental factors including the total ozone column amount, solar elevation, and depth in the ocean, as well as the presence of clouds, ice, and snow. Employing the radiative transfer model described above for the coupled atmosphere-sea ice-ocean system, and assuming total ozone column amounts of 400 DU and 200 DU, Hamre et al. (2008) computed $\overline{I}(\lambda)$ at the bottom of the snow-covered sea ice and at various depths of open water, and used the resulting $\overline{I}(\lambda)$-values in Eq. (9.23) to calculate the primary productivity. The results of this study may be summarized as follows:

- an ozone depletion increases not only harmful UVR, but also beneficial PUR;
- at high latitudes, the benefits of increased PUR for phytoplankton under sea ice and below a certain depth in the ocean dominates over the damage caused by increased UVR;
- a large fraction of the primary production in the polar regions is caused by ice algae growing in environments well protected from UVR;
- the primary production in the polar regions could increase by as much as 1% for a 50% ozone depletion.

9.4 Discussion and Conclusions

We have given a review of UV and visible radiative transfer in a CASIO system with an emphasis on basic physical principles. To illustrate applications of the theory we have:

(1) Compared two different models (based on the deterministic discrete-ordinate radiative transfer (DISORT) method and stochastic Monte Carlo simulations)

for radiation penetration into the open ocean, which for a given set of input parameters have been shown to give identical results. Compared measured and modeled radiative transfer in a CASIO system, which reveals that accurate transmittances, as well as accurate values for the radiative energy deposition versus depth, can be calculated using the CASIO-DISORT model.

(2) Discussed results of a study showing that multiple scattering in a highly scattering medium, such as sea ice, gives rise to a marked enhancement of the downward irradiance across the atmosphere-sea ice interface.

(3) Discussed results of a recent study of the primary production in icy polar waters, which, contrary to previous investigations, reveal that a 50% ozone depletion might lead to an increase (~1%) rather than a decrease in primary productivity.

In view of the above, we conclude that:

- for a CAO system, our ability to model the transport of UV radiation and visible light appears to be limited as much by reliable information about optical properties of marine constituents and atmospheric aerosol loading as by our ability to accurately solve the radiative transfer equation;
- multiple scattering in sea ice leads to a significant enhancement of the downward irradiance across the atmosphere-sea ice interface;
- it is important to make field measurements to provide reasonable input to modeling efforts; and
- in icy polar waters, an ozone depletion might lead to an increase rather than a decrease in primary productivity.

Acknowledgements

This work was supported by the US National Science Foundation and the Norwegian Research Council.

References

Anderson GP, Clough SA, Kneizys FX, Chetwynd JH, and Shettle EP (1987) AFGL Atmospheric Constituent Profiles (0-120) km, AFGL-TR-86-0110, AFGL (OPI), Hanscom AFB, MA

Anderson JG, Toohey DW, and Brune WH (1991) Free radicals within the Antarctic vortex: The role of CFCs in Antarctic ozone loss. Science 251: 39 – 46

Calkins J, and Thordardottir C (1980) The ecological significance of solar UV radiation on aquatic organisms. Nature 283: 563 – 566

Collins DG, Blattner WG, Wells MB, and Horak HG (1972) Backwards Monte Carlo calculations of the polarization characteristics of the radiation field emerging from spherical shell atmospheres. Appl. Opt. 11: 2684 – 2705

Cox GF, and Weeks WF (1983) Equations for determining the gas and brine volumes in sea-ice samples. J. Glaciol. 29: 306 – 316

Cullen JL, Neale PJ, and Lesser MP (1992) Biological weighting function for the inhibition of phytoplankton photosynthesis by ultraviolet radiation. Science 258: 646 – 650

Cullen JL, and Neale PJ (1994) Ultraviolet radiation, ozone depletion, and marine photosynthesis. Photosyn. Res. 39: 303 – 320

Deal CJ, Kieber DJ, Toole DA, Stamnes K, Jiang S, and Uzuka N (2005) Dimethylsulfide photolysis rates and apparent quantum yields in Bering Sea seawater. Continental Shelf Research 25: 1825 – 1835

Döhler G (1985) Effect of UV-B radiation (290 – 320 nm) on the nitrogen metabolism of several marine diatoms. J. Plant Physiol. 118: 391 – 400

Döhler G, and Hagmeier E (1997) UV effects on pigments and assimilation of 15N-ammonium and 15N-nitrate by natural marine phytoplankton of the North Sea. Bot. Acta 110: 481 – 488

Gerland S, Winther J-G, Ørbæk JB, and Ivanov BV (1999) Physical properties, spectral reflectance and thickness development of first year fast ice in Kongsfjorden, Svalbard. Polar Res. 18: 275 – 282

Gjerstad KI, Stamnes JJ, Hamre B, Lotsberg JK, Yan B, and Stamnes K (2003) Monte Carlo and discrete-ordinate simulations of irradiances in the coupled atmosphere-ocean system. Appl. Opt. 42: 2609 – 2622

Goes JI, Handa N, Taguchi S, Hama T, and Saito H (1995) Impact of natural ultraviolet radiation on production patterns and composition of dissolved free and combined amino acids in marine phytoplankton. J. Plankton Res. 17: 1337 – 1362

Gordon HR (1997) Atmospheric correction of ocean color imagery in the Earth Observing System era. J. Geophys. Res. 102: 17,081 – 17,106

Häder DP (ed) (1997) The effect of ozone depletion on aquatic ecosystems. R.G. Landes Company, Academic Press, Austin

Häder DP, Kumar HD, Smith RC, and Worrest RC (1998) Effects on aquatic ecosystems. J. Photochem. Photobiol. B: Biology 46: 53 – 68

Hamre B, Winther J-G, Gerland S, Stamnes JJ, and Stamnes K (2004) Modeled and measured optical transmittance of snow covered first-year sea ice in Kongsfjorden, Svalbard. J. Geophys. Res. 109:DOI:10.1029/2003JC001926

Hamre B, Stamnes JJ, Frette Ø, Erga SR, and Stamnes K (2008) Could stratospheric ozone depletion lead to enhanced aquatic primary production in the polar regions? Limnol. Oceanogr. 53: 332 – 338

Herman JR, Barthia PK, Ahmad Z, and Larko D (1996) UV-B radiation increases (1979 – 1992) from decreases in total ozone. Geophys. Res. Lett. 23: 2117 – 2120

Herman JR, McKenzie RL, Diaz SB, Kerr JB, Madronich S, and Seckemeyer G (1999) Ultraviolet radiation at the earth's surface. In: Scientific Assessment of Ozone Depletion: 1998 WMO Rep. 44, World Meteorol. Org., Global Ozone Res. Monit. Proj., Geneva, Switzerland, pp 9.1 – 9.46

Holm-Hansen O, Lubin D, and Helbling EW (1993a) Ultraviolet radiation and its effects on organisms in aquatic environments. In: Young AR, Björn LO, Moan J, Nultsch W (eds) Environmental UV Photobiology, Plenum Press, New York

Holm-Hansen O, Helbling EW, and Lubin D (1993b) Ultraviolet radiation in Antarctica: Inhibition of primary production. Photochem. Photobiol. 58: 567 – 570

Jiang S, Stamnes K, Li W, and Hamre B (2005) Enhanced Solar Irradiance Across the Atmosphere-Sea Ice Interface: A Quantitative Numerical Study. Appl. Opt. 44: 2613 – 2625

Jin Z, and Stamnes K (1994) Radiative transfer in nonuniformly refracting media such as the atmosphere/ocean system. Appl. Opt. 33: 431 – 442

Jin Z, Stamnes K, Weeks WF, and Tsay SC (1994) The effect of sea ice on the solar energy budget in the atmosphere-sea ice-ocean system: A model study. J. Geophys. Res. 99: 25281 – 25294

Jin Z, Charlock TP, Rutledge K, Stamnes K, Wang Y (2006) An analytical solution of radiative transfer in the coupled atmosphere-ocean system with rough surface. Appl. Opt. 45: 7443 – 7455

Jokiel PL, and York RH (1984) Importance of ultraviolet radiation in photoinhibition of microalgae growth. Limnol. Oceanogr. 29: 192 – 199

Karentz D, Cleaver JE, and Mitchell DL (1991) Cell survival characteristics and molecular responses of Antarctic phytoplankton to ultraviolet-B radiation. J. Phycol. 27: 326 – 341

Karentz D, McIntyre S, Matlick HA, Menzies D, Ondrusek M, Wan Z, and Waters KJ (1992) Ozone depletion: Ultraviolet radiation and phytoplankton biology in Antarctic waters. Science 255: 952 – 959

Legendre L, Ackley SF, Dieckmann GS, Gullicksen B, Horner R, Hoshiai T, Melnikov IA, Reeburgh WS, Spindler M, and Sullivan CW (1992) Ecology of sea biota: 2. Global significance. Polar Biol. 12: 429 – 444

Lenoble J (ed) (1985) Radiative Transfer in Scattering and Absorbing Atmospheres: Standard Computational Procedures. A. Deepak, Hampton, VA

Li W, Stamnes K, Spurr R, and Stamnes JJ (2008) Simultaneous retrieval of aerosols and ocean properties: A classic inverse modeling approach. Ⅱ. SeaWiFS Case Study for the Santa Barbara Channel. Int. J. Rem. Sens. DOI: 10.1080/01431160802007632, 29, 5689 – 5698

Lobman M, Döhler G, Huckenbeck N, and Verdini S (1998) Effects of UV radiation of different wavebands on pigmentation, 15N-ammonium uptake, amino acid pools and adenylate contents of marine diatoms. Mar. Biol. 130: 501 – 507

Mobley CD (1994) Light and water: radiative transfer in natural waters. Academic Press, San Diego, CA

Mobley CD, Gentili B, Gordon HR, Jin Z, Kattawar GW, Morel A, Reinersmann P, Stamnes K, and Stavn RH (1993) Comparison of numerical models for computing underwater light fields. Appl. Opt. 32: 7484 – 7504

Morel A (1974) Optical properties of pure sea water. In: Jerlov NG, Nielsen ES (eds) Optical Aspects of Oceanography, Academic Press, pp.1 – 24

Morel A (1991) Light and marine photosynthesis: A model with geochemical and climatological implications. Prog. Oceanogr. 26: 263 – 306

Morel A, and Gentili B (1991) Diffuse reflectance of oceanic waters: Its dependence on sun angle as influenced by the molecular scattering contribution. Appl. Opt. 30: 4427 – 4438

Morel A, and Maritorena S (2001) Bio-optical properties of oceanic waters: A reappraisal, J. Geophys. Res. 106: 7163 – 7180

Neale PJ, Cullen JL, Lesser MP, and Melis A (1993) Physiological bases for detecting and predicting photoinhibition of aquatic photosynthesis by PAR and UV radiation. In: Yamamoto

H (ed) Photosynthetic response to the environment. American Society of Plant Physiology, Rockville, pp.61 – 77

Neale PJ, Cullen JJ, and Davis RF (1998) Inhibition of marine photosynthesis by ultraviolet radiation: Variable sensitivity of phytoplankton in the Weddell-Scotia Confluence during the austral spring, Limnol. Oceanogr. 43: 433 – 448

Pegau WS, Cleveland JS, Doss W, Kennedy CD, Maffione RA, Mueller JL, Trees CC, Weidemann AD, Wells WH, and Zaneveld JRV (1995) A comparison of methods for the measurement of the absorption coefficient in natural waters. J. Geophys. Res. 100: 13,201 – 13,220

Perovich DK, and Maykut GA (1996) Solar heating of a stratified ocean in the presence of a static ice cover. J. Geophys. Res. 95: 18,233 – 18,245

Pope RM, and Fry ES (1997) Absorption spectrum (380 – 700 nm) of pure water, Ⅱ, Integrating cavity measurements. Appl. Opt. 36(33): 8710 – 8723

Prézelin BB, Boucher NP, and Smith RC (1994) Marine primary production under the Antarctic ozone hole. In: Weiler S, Penhale P (eds) Ultraviolet Radiation and Biological Research in Antarctica, Antarctic Research Series 62: 159 – 186

Rottman GJ, Woods TN, and Sparn TP (1993) Solar stellar irradiance comparison experiment I. Instrument design and operation. J. Geophys. Res. 98: 10,667 – 10,678

Slaper H, Velders GJM, Daniel JS, de Gruijl FR, and van der Leun JC (1995) Estimates of ozone depletion and skin cancer to examine the Vienna Convention achievements. Nature 384: 256 – 259

Smith RC, and Baker KS (1989) Stratospheric ozone, middle ultraviolet radiation and phytoplankton productivity. Oceanogr. Mag. 2: 4 – 10

Smith RC, Prezelin BB, Baker KS, Bidigare RR, Boucher NP, Coley, T, Karentz D, Maclntyre S, Matlick HA, Menzies D, Ondrusek M, Wan Z and Waters KJ (1992) Ozone depletion: Ultraviolet radiation and phytoplankton biology in Antarctic waters. Science 255: 952 – 957

Solomon S (1990) Progress towards a quantitative understanding of Antarctic ozone depletion. Nature 347: 347 – 354

Stamnes K, Tsay S-C, Wiscombe WJ, and Jayaweera K (1988) Numerically stable algorithm for discrete-ordinate-method radiative transfer in multiple scattering and emitting layered media. Appl. Opt. 27: 2502 – 2509

Stamnes K, Tsay S-C, Wiscombe WJ, and Laszlo I (2000) DISORT, A General-Purpose Fortran Program for Discrete-Ordinate-Method Radiative Transfer in Scattering and Emitting Layered Media: Documentation of Methodology, Report. ftp://climate1.gsfc.nasa.gov/wiscombe/

Stamnes K, Li W, Yan B, Eide H, Barnard A, Pegau WS, and Stamnes J (2003) Accurate and self-consistent ocean color algorithm: simultaneous retrieval of aerosol optical properties and chlorophyll concentrations. Appl. Opt. 42: 939 – 951

Thomas GE, and Stamnes K (1999) Radiative Transfer in the Atmosphere and Ocean. Cambridge University Press

Vasilkov A, Krotkov N, Herman J, McClain, K. Arrigo C, and Robinson W (2001) Global mapping of underwater UV irradiances and DNA-weighted exposures using Total Ozone Mapping Spectrometer and Sea-viewing Wide Field-of-view Sensor data products. J. Geophys Res. 106: 27202 – 27219

Wängberg S-Aa, Garde K, Gustavson K, and Selmer J (1999) Effects of UV-B radiation on marine phytoplankton communities. J. Plankton Res. 21: 147 – 166

Wheeler PA, Gosselin M, Sherr EE, Thibault D, Kirchman DL, Benner R, and Whitledge TE (1996) Active cycling of organic carbon in the central Arctic Ocean. Nature 380: 697 – 699

Worrest RC (1986) The effect of solar UV-B radiation on aquatic systems: An overview. In: Titus JG (ed) Effects of Changes in Stratospheric Ozone and Global Climate, Overview. U.S. Environmental Protection Agency and United Nations Environmental Program 1, pp.175 – 191

Zeebe RE, Eicken H, Robinson DH, and Wolf-Gladrow D (1996) Modeling the heating of melting sea ice though light absorption by microalgae. J. Geophys. Res. 101: 1163 – 1181

Zeng J, Jin Z, and Stamnes K (1993) Impact of stratospheric ozone depletion on UV penetration into the ocean at high latitudes. In: Underwater Light Measurements. Proc. SPIE 2048: 56 – 63

Zerefos CS, and Bais AF (eds) (1997) Solar Ultraviolet Radiation: Modeling, Measurements and Effects. Springer-Verlag, Berlin